Catal Lett (2014) 144:1450–1459
DOI 10.1007/s10562-014-1285-6

Vapor Phase Oxidation of Benzyl Alcohol Over Gold Nanoparticles Supported on Mesoporous TiO_2

Ashish Kumar · Vanama Pavan Kumar · Balla Putra Kumar · Venkataraman Vishwanathan · Komandur V. R. Chary

Received: 22 April 2014 / Accepted: 22 May 2014 / Published online: 10 June 2014

Abstract The vapor phase oxidation of benzyl alcohol was investigated over gold nanoparticles supported on mesoporous titanium dioxide (anatase) catalysts under aerobic conditions. The catalysts were prepared by homogeneous deposition–precipitation method using urea as the precipitating agent. The physico-chemical properties of the synthesized catalysts were investigated by X-ray diffraction (XRD), transmission electron microscopy (TEM), pore size distribution (PSD), CO-chemisorption and X-ray photoelectron spectroscopy (XPS) techniques. The crystallite size of gold in Au/TiO_2 catalysts was measured from XRD. The mesoporosity of TiO_2 support and Au/TiO_2 catalysts were confirmed by PSD analysis. TEM results suggest that gold nanoparticles are well dispersed over mesoporous TiO_2. The catalytic functionality is well substantiated with particle size measured from TEM. XPS results reveal the formation of Au(0) after chemical reduction by $NaBH_4$. The vapor phase benzyl alcohol oxidation was used as a test reaction to investigate the influence of the metal, nature of the support, and of metal-support interactions in Au/TiO_2 catalysts and also the catalytic activity and stability of the Au/TiO_2 catalysts. The conversion of benzyl alcohol was found to increase with decrease in the size of gold particles. Smaller gold particles and a higher amount of small gold particles had a beneficial effect on the catalytic activity. The catalytic activity in the presence of oxygen is believed to be associated with the transport of electrons through the catalyst to the adsorbed oxygen on the surface.

Keywords Gold nanoparticles · Mesoporous TiO_2 (anatase) · Benzyl alcohol oxidation · Benzaldehyde

1 Introduction

Catalytic oxidation of alcohols to the corresponding carbonyl compounds is of great importance in both the basic and applied research due to the utilization of carbonyl compounds as versatile intermediates for the synthesis of fine chemicals [1, 2]. Extensive research work both in fundamental and in applied catalysis has been carried out in order to understand the catalytic properties of gold nanoparticles supported on mesoporous titanium dioxide, prepared by homogeneous deposition–precipitation (HDP) method using urea as the precipitating agent. It is well established that the catalytic activity of supported gold nanoparticles depends on the particle size, the nature of support and the preparation method. For example, nanogold particles supported on reducible oxides like CeO_2, TiO_2 and Fe_2O_3 [1, 2] are more active and stable than that are supported on non-reducible oxides (SiO_2, Al_2O_3 etc.).

Among the reactions studied, the vapor phase oxidation of benzyl alcohol (BzOH) to benzaldehyde (PhCHO) is commercially of importance since the process is environmentally benign and needs less expensive additives. Conventionally, benzaldehyde is produced as a by-product during the oxidation of toluene ($PhCH_3$) to benzoic acid (PhCOOH) or from the hydrolysis of benzyl dichloride. These routes are said to generate a large amount of environmentally hazardous by-products like organic chlorine or

A. Kumar · V. P. Kumar · B. P. Kumar · K. V. R. Chary (✉)
Catalysis Laboratory, Inorganic & Physical Chemistry Division, CSIR-Indian Institute of Chemical Technology, Hyderabad 500 007, India
e-mail: kvrchary@iict.res.in

V. Vishwanathan
Department of Chemistry, Sreyas Institute of Engineering and Technology, Hyderabad 500068, India

benzoic acid. Hence, this limits the usage of benzaldehyde as an intermediate in the production of cosmetics, pharmaceutical, fine chemicals and flavouring industries [3, 4]. From the commercial view, air/molecular oxygen is the favourable choice as the primary oxidant since they produce water as only the by-product [5]. However, the use of air requires the development of newer and novel catalysts in order to achieve higher catalytic activity under ambient reaction conditions. Many studies have employed supported gold as catalysts in several catalytic applications including selective aerobic oxidation of alcohols such as benzyl alcohol [5–7]. In order to achieve a high catalytic performance, these catalysts are used in the form of nanocomposites where nanoparticles of gold are loaded onto the support materials like activated carbon, metal oxides and polymers. However, such batch reactions in liquid phase require a long period of time to reach the steady state and also require the separation of catalysts from the products. From the viewpoint of atom economy and green chemistry, more emphasis has been laid on the vapor phase catalytic oxidation of benzyl alcohol to benzaldehyde [3, 4, 7–11] since it is solvent free continuous system and provides a high quality of benzaldehyde and the toluene selectivity reduced substantially at the cost of conversion. Recently, Rossi and co-workers have reported that gold catalysts to be more effective in the vapor phase oxidation of volatile alcohols to form the corresponding ketones and aldehydes [3, 4, 9]. Metal catalysts containing supported—Pd, Cu and Co have been studied for the title reaction. However, their catalytic activities were found to be much lower compared to supported gold catalyst [10, 11].

Titanium dioxide (TiO_2) is a known reducible oxide support having various applications. To name of few–they are used in solar energy conversion, gas sensors, waste water treatment, water splitting, water purification, and carbon dioxide conversion and so on. The importance of TiO_2 is selectively due to its low cost, good chemical and mechanical stability, high catalytic activity and non-toxic nature, strong metal-support interaction in TiO_2–supported catalysts [12–14]. As a support material, it reduced the gold ions at the metal support interface [15]. The other feature is the conduction band of anatase can also transfer the electrons of the excited gold to adsorb O_2 to form active superoxide radical anions [16]. Mesoporous TiO_2, as support material, shows a high efficiency due to its large surface area. However, there are great challenges in preparing mesoporous TiO_2 having large surface area and high crystallinity.

Some of the reported values [17] of BET surface area of the mesoporous TiO_2 are in the range of 80–100 m^2/g. This is much smaller than the amorphous TiO_2 forms. Several techniques, such as sol–gel method, chemical vapor deposition, laser vaporization, modified impregnation, precipitation-reduction, and photo-reduction, have been developed to design and modulate the Au/TiO_2 catalysts. One of the preferred and versatile methods is the HDP method using urea as the precipitating agent. This has many advantages like requirement of simple equipment, better control of pore structures, and the availability of higher dispersion of gold particles at lower concentration on the catalyst support [18]. Nano-sized gold particles have been reported to show a higher catalytic activity [19–21]. The present investigation deals with a direct correlation study between dispersion, metal area and oxidation of benzyl alcohol to benzaldehyde over supported gold nanoparticles. This work has allowed us to draw clear conclusions regarding (i) the quantitative influence of particle composition; (ii) the role of particle size; and (iii) the influence of the support on benzyl alcohol activity. The structural features of Au/TiO_2 catalysts were investigated by X-ray diffraction (XRD), CO-chemisorption, Brunauer–Emmet–Teller (BET), nitrogen adsorption–desorption and BJH pore size distribution (PSD), transmission electron microscopy (TEM), and X-ray photoelectron spectroscopy (XPS).

2 Materials and Methods

2.1 Catalyst Preparation

2.1.1 Preparation of Mesoporous TiO_2 Support

In a typical synthesis of mesoporous TiO_2 [22], titanium hydroxide was prepared by the hydrolysis of titanium isopropoxide from a mixture of 2-propanol and water at room temperature under vigorous stirring for 1 h. The molar ratios were investigated as Ti/2–propanol/H_2O equal to 1:22:5; volume (mL) ratios 10:60:3. The precipitate was aged at 80 °C and subsequently dried in a hot air oven at 100 °C. Finally, the dried sample (mesoporous TiO_2) was calcined at 400 °C for 4 h at a heating rate of 1 °C/min.

2.1.2 Preparation of Gold Catalysts

The Au/TiO_2 catalysts with varying gold loadings were prepared by HDP method using urea as the precipitating agent [18, 23]. The mixture of an aqueous solution containing $HAuCl_4.3H_2O$ (Sigma-Aldrich, 99.8 %, with desired gold loading) and urea was stirred with gradual heating to a temperature up to 95 °C for 6 h. On heating, the urea decomposes to ammonia and hence the precipitation occurs in a homogeneous way in the whole bulk solution as the pH shift towards basic conditions (pH $\sim$ 6–8). Subsequently, the support (mesoporous TiO_2) was added to the above solution with continuous stirring.

The requisite amount of 0.1 M freshly prepared $NaBH_4$ aqueous solution [24] was added to the above solution so as to precipitate metallic gold nanoparticles on TiO_2 support. The solid product formed was filtered, washed thoroughly with deionized water until the filtrate contained no chloride ions (confirmed with $AgNO_3$ test) and subsequently dried in hot air oven for 5 h and finally calcined at 400 °C for 3 h in N_2 atmosphere. The EDAX–analysis suggest that the concentration of sodium is present in negligible amount (<0.01 %).

2.2 Catalyst Characterization

X-ray powder diffraction (XRD) patterns of the catalysts were recorded on a Rigaku Miniflex (M/s. Rigaku Corporation, Japan). X-ray diffractometer using Ni filtered CuKα radiation ($\lambda = 0.15406$ nm) with a scan speed of 2° min^{-1} and a scan range of 10°–80° for wide angle diffraction at 30 kV and 15 mA. The crystallite size of gold is calculated by using Debye–Scherrer equation and phase identification with the help of the JCPDS files.

The CO-chemisorption measurements were carried out on AutoChem 2910 (Micromeritics, USA) instrument. A 100 mg of the catalyst was pretreated with He gas for 1 h at 150 °C. The sample was subsequently cooled to 50 °C in the same He gas stream. CO uptake was determined by injecting pulses of 10 % CO/He from a calibrated online sampling valve into the He gas stream passing over the samples at 80 °C. Metal area, metal dispersion and metal average particle size were calculated assuming the stoichiometric factor (CO/Au) as 1. Adsorption was deemed to be completed after three successive runs showed similar peak area.

Gold content was determined by inductively coupled plasma optical emission spectrometer (ICP–OES) on a Varian 720-ES instrument. Solid samples were first digested in a mixture of HF, HCl, and HNO_3 in a microwave oven for 2 h and further diluted with deionised water to analyze the gold contents by ICP–OES. ICP analysis, performed on the fresh samples of Au/TiO_2 catalysts.

The BET surface areas of the catalysts were obtained from N_2 adsorption–desorption isotherms (Autosorb1-Quantachrome instruments, USA at −196 °C). The samples were first out gassed at 300 °C to ensure a clean surface prior to construction of adsorption isotherm. The Barrett–Joyner–Halenda (BJH) method was used to calculate the pore-size distribution from the desorption branch of the isotherm (Autosorb1-Quantachrome, USA).

Transmission electron microscope (TEM) images of the catalysts were obtained using a Technai-12, FEI, Netherlands at an accelerating voltage of 120 kV. The specimens were prepared by dispersing the samples in methanol using an ultrasonic bath and evaporating a drop of resultant suspension onto the carbon coated copper grid.

XPS was used to study the chemical composition and oxidation state of catalyst surfaces. The XPS spectra of the catalysts were measured on a XPS spectrometer (KRATOS Axis 165, Shimadzu, UK) with MgKα radiation 1253.6 eV at 75 W. The gold 4*f* core-level spectra were recorded and the corresponding binding energies referenced to the C 1s line at 284.6 eV (accuracy within (0.2 eV)). The background pressure during the data acquisition was kept below 10^{-9} torr.

2.3 Catalytic Activity

The vapor phase oxidation of benzyl alcohol was carried out in a fixed bed vertical down flow glass reactor (length = 520 mm, i.d. = 12 mm) under ambient atmospheric pressure. An amount of 1.0 g catalyst was diluted with an equal amount of quartz grains of similar size was packed in between two layers of quartz wool. The upper portion of the reactor is filled with glass beads which serve as a preheater for the reactant. Prior to the oxidation reaction, each catalyst was activated at 250 °C for 2 h in the presence of N_2 flow (50 mL/min). Thereafter, the benzyl alcohol (Sigma-Aldrich, 99.8 %) was fed into the reactor in a stoichiometric quantity (WHSV = 2.8428 h^{-1}) using a syringe pump (Perfusor, B. Braun, Germany) by passing air along with the reactant at 320 °C. The reaction products were collected in an ice-cold trap at the bottom of the reactor for every 1 h.

The reaction products were analyzed by a HP-6890 gas chromatograph equipped with a HP-5 capillary column having flame-ionization detector (FID) and the reaction products were also identified by HP-5973 quadruple GC–MSD system with a HP-1MS capillary column using He as a carrier gas. However, the gaseous products were introduced to a 1 cm^3 gas sampler and analyzed by gas chromatography (SHIMADZU GC–2014) equipped with a thermal conductivity detector (TCD) using Carboxen 1000 column, under an Helium as carrier gas.

3 Results and Discussion

3.1 Characterization of Catalysts

The powder XRD patterns of various loadings of gold containing mesoporous TiO_2 catalysts are shown in Fig. 1. The Bragg diffraction peaks at $2\theta \sim 25.6°$, 37.8°, 48.1°, 55.1°, and 62.7° which are indexed to (101), (112), (200), (105) and (204) respectively, are the characteristic reflections of anatase phase of mesoporous TiO_2 (JCPDS file number: 21-2172) [25]. However, the mesoporous ordered

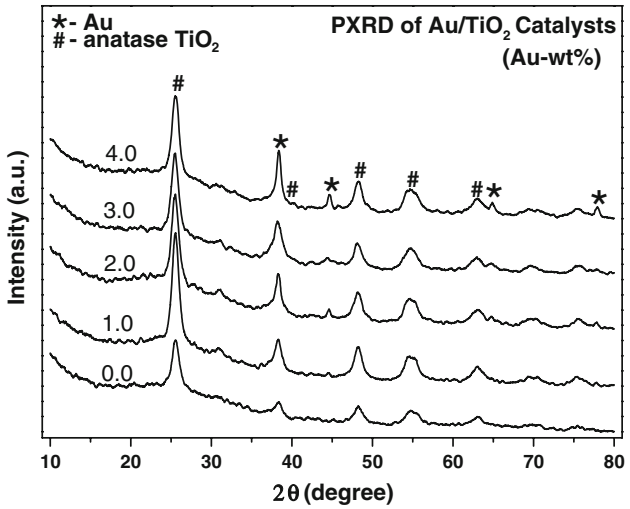

Fig. 1 Powder XRD patterns of mesoporous TiO_2 and Au/TiO_2 catalysts (fresh)

Table 1 The physico-chemical properties of various Au/TiO_2 catalysts

Au loading (wt%)	CO_{irr} (μmol/g)	CO/Au	A_m^a (m^2/g_{cat})	d_{Au}^b (nm)	TOF/10^{-3} (s^{-1})	d_{Au}^c (nm)
1.0	8.51	0.1676	0.4462	6.96	208	8.89
2.0	15.07	0.1484	0.7892	7.87	141	9.61
3.0	20.78	0.1364	1.0884	8.56	76	10.18
4.0	24.53	0.1208	1.2848	9.67	61	12.86

[a] Metal area (per catalyst)

[b] Au Particle size determined from CO_{irr} uptake values

[c] Au Crystallite size determined from XRD

structure of TiO_2 could be retained even after complete gold deposition, as shown in the Fig. 1. With increasing gold content in Au/TiO_2 catalysts, the intensities of anatase peaks steadily become weaker and the width of the diffraction peaks ($2\theta = 25.6°$) of anatase slightly became wider. This was probably due to the fact that gold nanoparticles suppress the crystallization of TiO_2. It was found that anatase TiO_2 phase is thermally stable and the crystal size apparently is not affected when the gold nanoparticles deposited onto TiO_2 support, because the full width at half maximum is (FWHM) very similar in both diffractograms (TiO_2 (112) and Au (111)).

The Au/TiO_2 catalysts exhibits four diffraction peaks at $2\theta \sim 38.2°$, 44.6°, 64.9°, 77.9° which are indexed to (111), (200), (220), and (311) reflections, respectively, for the face-cantered cubic (FCC) lattice structure of gold (JCPDS file number: 04-0784) [26]. A considerable increase in the line widths, with varying gold content

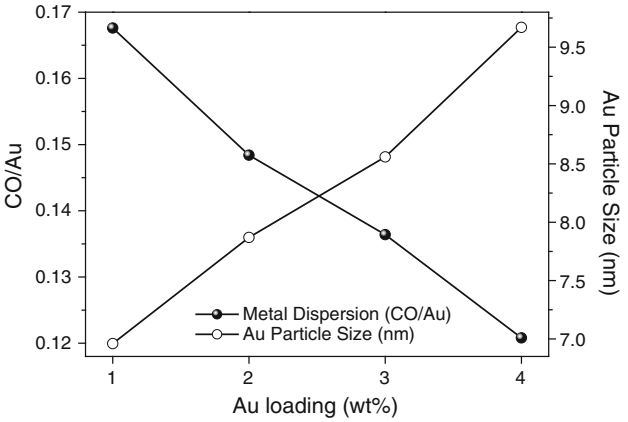

Fig. 2 Effect of CO-chemisorption properties on Au (wt%) loadings

(1.0–4.0 wt%) is a feature arising due to decrease in particle size. The peaks are sharp and intense indicating good crystallinity of metallic gold. The crystallite size of gold were calculated from the diffraction peak (111), by applying the Debye–Scherrer formula and reported in Table 1.

The physico-chemical properties of Au/TiO_2 catalysts such as dispersion, metal area and particle size were determined from CO-chemisorption and reported in Table 1. It is observed that increase in CO uptake with increase in metal loading leads to be an increase in particle size as shown in Fig. 2. This suggest to the agglomerization of gold particles at higher metal loading. This agglomerization in turn leads to the decrease in metal dispersion and increase in particle size with increase of gold loading and also decrease in catalytic reactivity in term of TOF (Table 1).

The nitrogen adsorption/desorption isotherms of mesoporous TiO_2 and various loadings of Au/TiO_2 catalysts are shown in Fig. 3a. All the samples exhibit Langmuir type IV isotherms [27, 28] which is a characteristic feature of mesoporous materials. The isotherms of all Au/TiO_2 catalysts are identical to the isotherm of mesoporous TiO_2 (Fig. 3a). The nitrogen adsorption isotherms of mesoporous TiO_2 and Au/TiO_2 catalysts exhibit H2-type hysteresis loop corresponding to pores with narrow necks and wider bodies [29] and features a sharp step in the P/P_0 range of 0.6–0.9, the sharpness of this step is indicative of the uniformity of the pore size [28], However, the hysteresis loops of all Au/TiO_2 catalysts become smaller, and position of the step shifts towards lower relative pressure in the range of 0.45–0.89 (as observed from the Fig. 3a), indicating that a smaller pore size is formed. This could be due to the deposition of gold nanoparticles in the pore of the mesoporous TiO_2. The calcinations temperature of 400 °C in the mesoporous TiO_2 sample is really important to lead

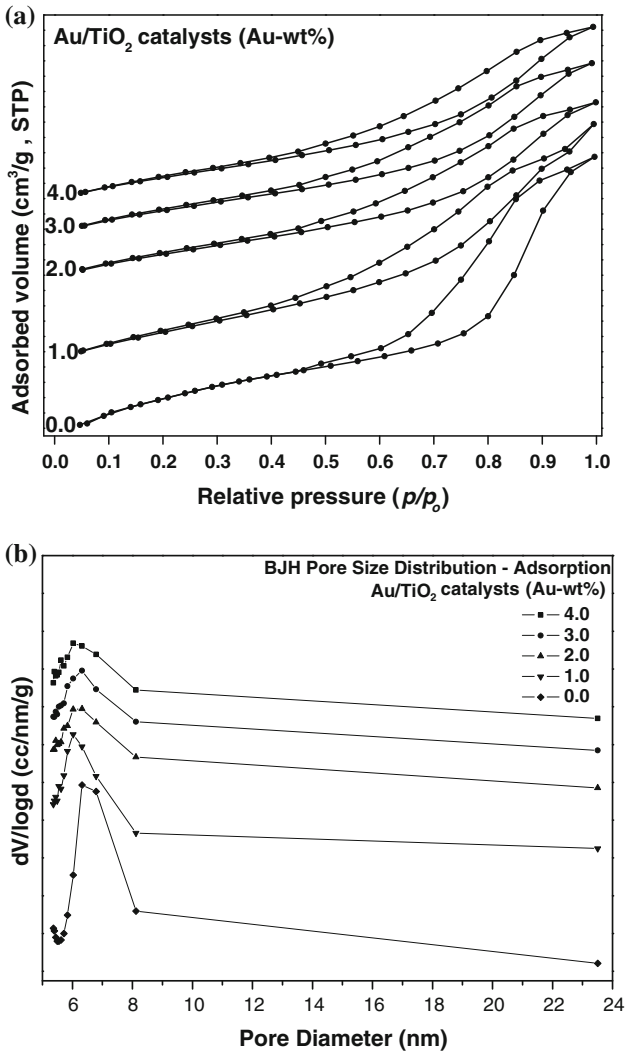

Fig. 3 **a** N_2 adsorption–desorption isotherms for mesoporous TiO_2 and various Au/TiO_2 catalysts, **b** BJH pore size distribution for mesoporous TiO_2 and various Au/TiO_2 catalysts

to a better mesoporous structure formation. The mean pore diameter of mesoporous TiO_2 and Au/TiO_2 catalysts are effectively the lowest one, obtained by the BJH method from the corresponding adsorption–desorption data are reported in Table 2.

The obtained surface areas are in agreement with those reported by other authors [30]. Physical properties/structural parameters of the samples derived from the nitrogen isotherms and the pore size distribution calculated from adsorption branch are shown in Fig. 3b. The surface area and pore volume decreases as a result of incorporation of gold nanoparticles into the mesoporous channels of the support [31].

TEM is a powerful technique to investigate the particle size of metal nanoparticles on catalytic support. The gold nanoparticles are spherical in shape and are highly dispersed and confined to the channels of the mesoporous TiO_2 as shown in Fig. 4. The corresponding histogram (Fig. 4) shows the distribution of gold particles of different loading of the catalysts. The mean diameter of gold particles is found to be ~7–12 nm (from TEM) while the average crystallite size of gold particles were obtained to be ~8–13 nm from XRD results.

In order to verify the oxidation states of gold element in as synthesized Au/TiO_2 catalysts were investigated by XPS. As can be seen from Fig. 5 the high resolution XPS spectrum shows binding energy of Au $4f_{7/2}$ at 84.0 and Au $4f_{5/2}$ at 87.7 eV, which are significantly different from Au^+ $4f_{7/2}$ (84.6 eV) and Au^{3+} $4f_{7/2}$ (87.0 eV). The result suggests that the gold species is in the metallic state [32] and these binding energy values correspond to the metallic gold particles [33]. However, the XPS results confirmed the absence of any contamination from sodium and chlorine species [24]. These results further confirm that gold nanoparticles on the surface of mesoporous TiO_2 support are in zero valence state. The XPS spectra of the present investigation did not show any peaks corresponding to the binding energies at 84.6 eV ($4f_{7/2}$) and 87.0 eV ($4f_{7/2}$) due to the cationic form of Au^+ and Au^{+3} oxidation states respectively. This suggests that the formation of gold metal nanoparticles takes place on the surface of mesoporous TiO_2 support.

Table 2 Textural properties and product selectivity (%) of mesoporous TiO_2 and different wt% of Au/TiO_2 catalysts

Au loading (wt%)	Au content [a] (wt %)	Surface area (m^2/g)	V_t (cc/g)	D_{BJH} (nm)	Products selectivity (%)		
					PhCOOH	PhH	$PhCH_3$
0.0	0.00	184	0.3201	6.937	–	–	–
1.0	0.89	166	0.2814	6.757	0.07	0.13	0.08
2.0	1.57	135	0.2117	6.374	0.01	0.08	0.01
3.0	2.46	133	0.2098	6.274	0.05	0.14	0.05
4.0	3.41	127	0.2029	6.235	0.06	0.17	0.06

BET method, V_t total pore volume, $D_{BJH,}$ average pore diameter calculated by BJH adsorption method

[a] Gold content measured by ICP–OES

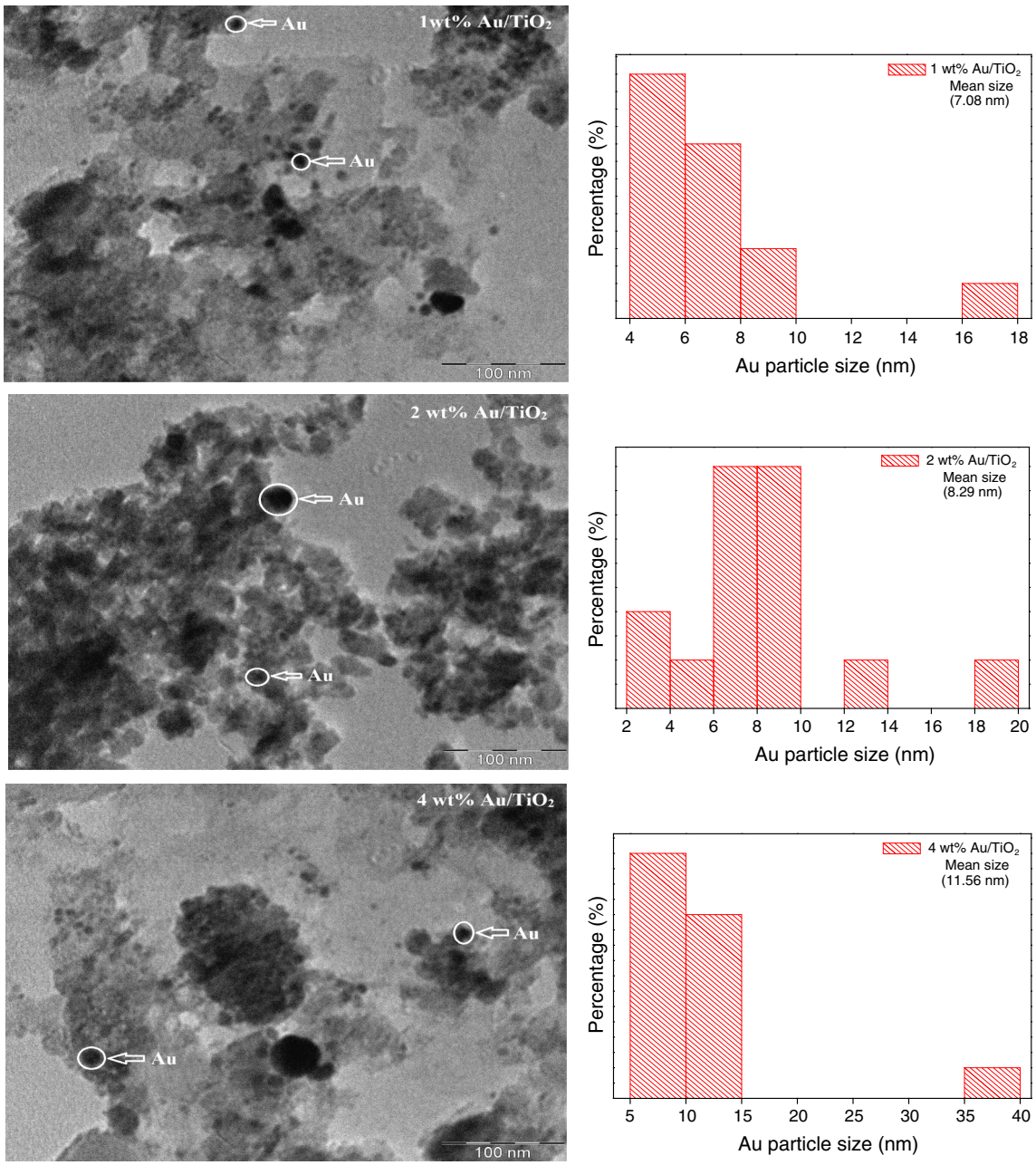

Fig. 4 TEM images and Histograms comparing the gold particle size distribution of different wt% of Au/TiO_2 catalysts (fresh)

3.2 Vapor Phase Oxidation of Benzyl Alcohol

3.2.1 Activity

The selective vapor phase oxidation of benzyl alcohol (BzOH) to benzaldehyde (PhCHO) with air as oxidant is employed to examine the catalytic performance of the Au/TiO_2 catalysts. In the absence of catalysts, only 5.7 % of benzyl alcohol was converted due to non-catalytic oxidation. The pure mesoporous TiO_2 support has shown very poor catalytic activity under the similar experimental condition.

The catalytic activity in terms of BzOH conversion and selectivity for PhCHO over Au/TiO_2 catalysts with different gold loadings (1–4 wt%) are shown in Fig. 6. As the gold loading increases, the conversion of BzOH and selectivity for PhCHO increases up to 2 wt% and further increase with loading shows a decrease in catalytic activity.

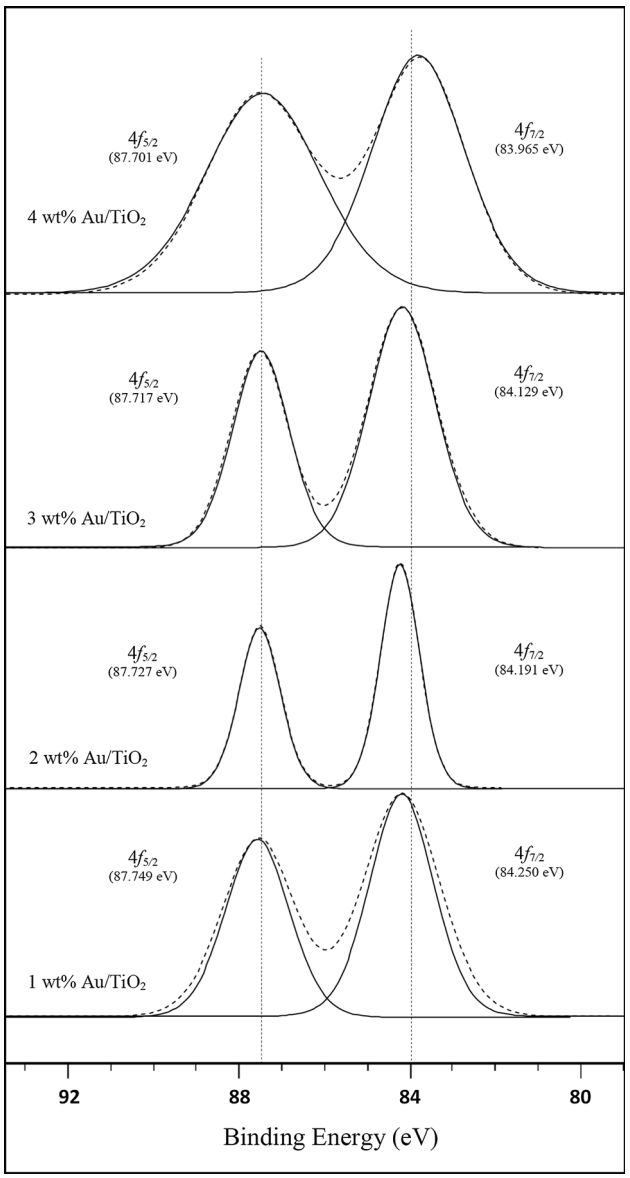

Fig. 5 XPS spectrum of Au/TiO_2 catalysts with different Au (wt%) loadings

The decrease in the conversion is probably due to less number of active metal sites of gold available on the mesoporous TiO_2 surface. This may be due to agglomerization of gold nanoparticles as evidenced from XRD and TEM results.

To understand the effect of BzOH activity in term of turnover frequency (TOF) against metal loading, a plot of turnover frequency (TOF) versus gold loading is shown in Fig. 7. TOF is defined as the number of BzOH molecules converted per active site of surface gold per second. The enhanced catalytic activity at lower loading was probably attributed to high dispersion of gold having smaller particle size on the mesoporous nature of the TiO_2 support.

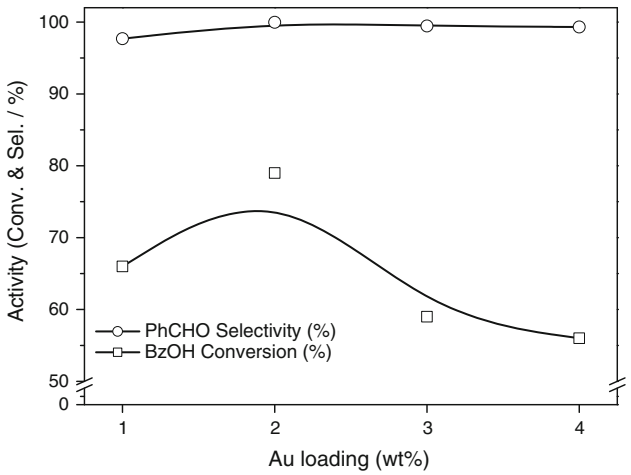

Fig. 6 Effect on BzOH conversion and selectivity for PhCHO over Au/TiO_2 catalysts with different gold loadings, reaction conditions: weight of the catalyst = 1.0 g; reaction temperature = 320 °C; WHSV = 2.8428 h^{-1}

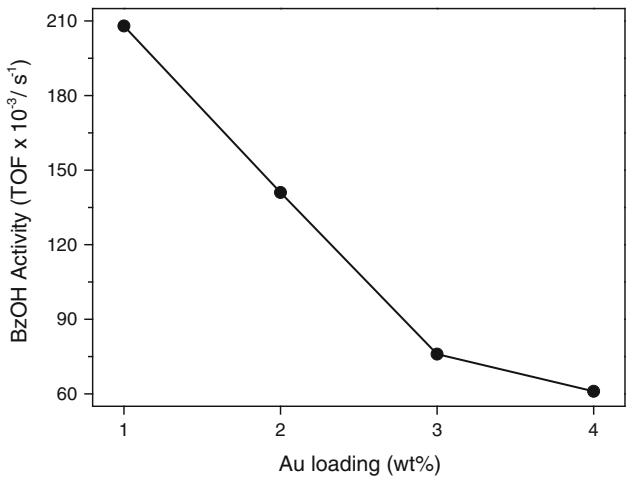

Fig. 7 Effect of BzOH activity in term of turnover frequency (TOF) with different gold loadings, reaction conditions: weight of the catalyst = 1.0 g; reaction temperature = 320 °C; WHSV = 2.8428 h^{-1}

3.2.2 *Deactivation*

The effect of temperature on the vapor phase oxidation of BzOH was investigated at different temperatures in the range 280 – 360 °C over Au/TiO_2 catalysts are shown in Fig. 8. The results suggest that below 280 °C no BzOH oxidation take place and over 360 °C the product underwent degradation with agglomerization of gold nanoparticles [3, 4]. As can be seen at the reaction temperature of 320 °C, BzOH conversion increases up to 79 % and PhCHO selectivity ($\approx$ 100 %) is found to be independent of reaction temperature. Therefore, the effect of reaction

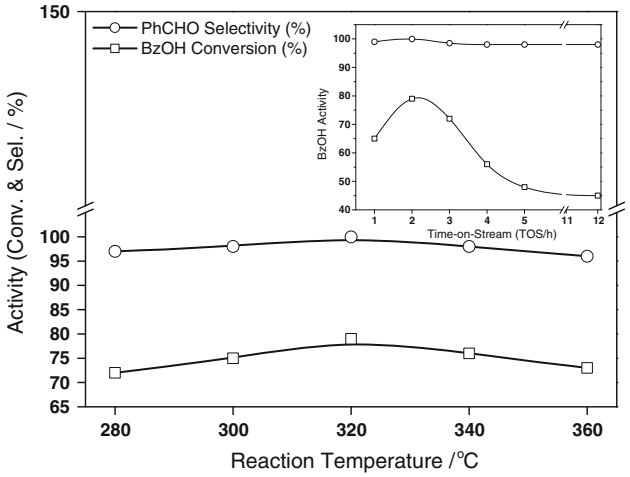

Fig. 8 BzOH activity over 2 wt% Au/TiO_2 catalyst, reaction conditions: weight of the catalyst = 1.0 g; WHSV = 2.8428 h^{-1}

temperature on catalytic properties suggest that high temperature favours for the complete oxidation of BzOH into benzoic acid (PhCOOH) and trace amount of benzene (PhH) and toluene ($PhCH_3$) as by-products [7, 34–38]. We found minute amounts of by-products in the product mixture (Table 2). However, the toluene selectivity is negligible <0.1 % over various Au loaded TiO_2 catalysts. Hence, the temperature (320 °C) was considered as the optimum reaction temperature and also referred as trade-off between PhCHO selectivity and BzOH conversion. In order to estimate the catalyst life in the present study the time on stream analysis was done at optimum reaction temperature of 320 °C. The gas analysis suggests that CO, CO_2 were not detected under the reaction condition (in the range of reaction temperature up to 320 °C).

The time on stream analysis on Au/TiO_2 catalysts were investigated to understand the stability of catalysts during benzyl alcohol oxidation reaction and is shown in Fig. 8 (inset). The conversion of BzOH and the product selectivity were monitored at different reaction intervals. As illustrated in Fig. 8 (inset), BzOH conversion (79 %) and PhCHO selectivity (99.97 %) obtained at 2 h was maximum over 2 wt% Au/TiO_2 catalyst and after allowing the reaction to last for 12 h, the BzOH conversion remained at 50 % and PhCHO selectivity remained at 90 % were determined.

To find an explanation for the faster deactivation of the above catalyst, we have done the TEM analysis of fresh and spent catalyst as shown in Fig. 9. These results suggest

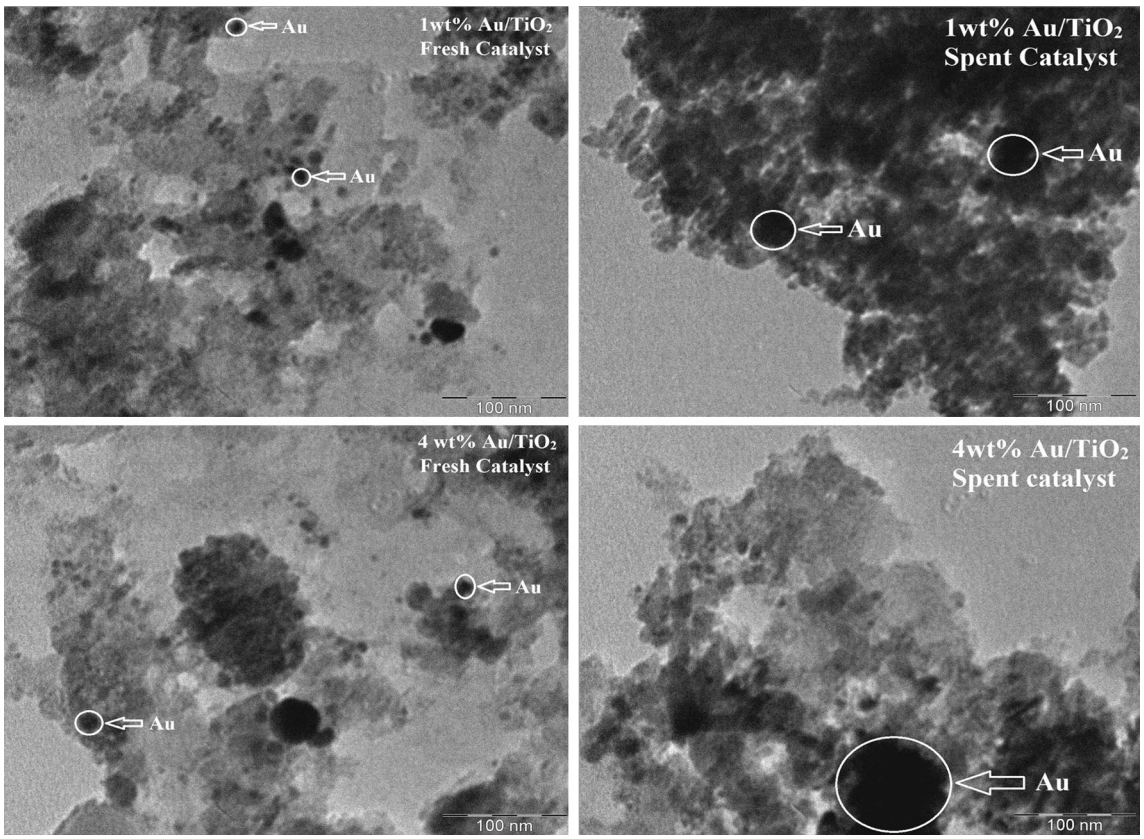

Fig. 9 TEM images of 1 wt% Au/TiO_2 and 4 wt% Au/TiO_2 catalysts (fresh/Spent)

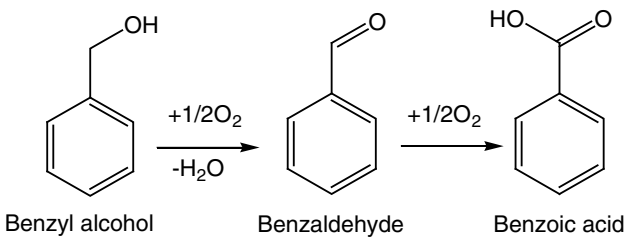

Scheme 1 Reaction pathway for the catalytic oxidation of benzyl alcohol to benzaldehyde over Au/TiO_2 catalysts

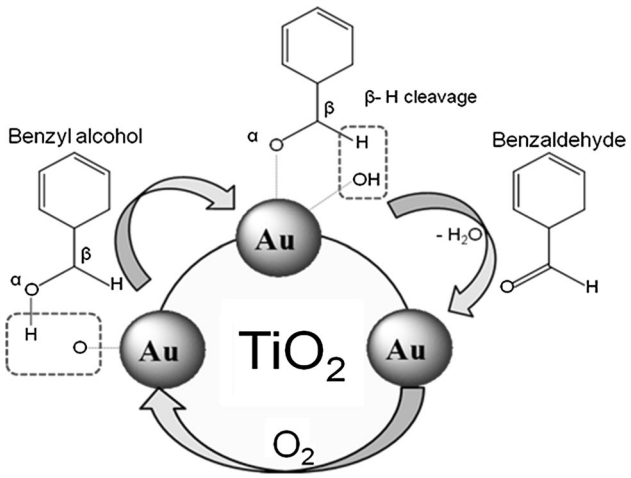

Scheme 2 Proposed reaction mechanism for the catalytic oxidation of benzyl alcohol to benzaldehyde over Au/TiO_2 catalysts

that the particle size of gold becomes larger during the reaction causing the deactivation or due to carbon deposition over Au/TiO_2 catalysts. To confirm this, an experiment has carried out the spent catalyst (after the reaction run 360 °C) which was recalcined at 300 °C for 4 h in air. On this sample a fresh experiment was carried under the similar reaction condition (WHSV = 2.8428 h^{-1} and T = 320 °C). We found the activity was much lower than the fresh reaction run under the aforementioned conditions.

The carbon balance of the fresh and spent catalysts was measured by CHNS analyser. No detectable amount was observed with fresh catalysts, whereas as a minute amount of carbon (<0.1 %) was deposited on the spent catalysts during the benzyl alcohol oxidation reaction.

The major product obtained was PhCHO with only minor concentration of PhCOOH as a by-product; indicates that the oxidation of BzOH occurs within the consecutive reactions and as represented in Scheme 1.

The supported gold catalyst needs contact time (at least 2 h) to reach its optimal catalytic activity. The presence of contact time indicates that the metallic gold nanoparticles on the catalyst surface are required to be activated at the initial stage and the oxygen molecules adsorbed on the metallic gold surface.

Further it is dissociated to create an oxidized gold surface for the oxidation of benzyl alcohol and a possible mechanism was proposed (Scheme 2), key features of which were the modes of interaction of benzyl alcohol molecules with the catalyst/support surfaces (chemisorption on the metal through C–H or O–H bond cleavage; binding to the support involving hydrogen bonding) and the concerted nature of the bonding changes during reaction [37]. The proposed mechanism for the oxidation of benzyl alcohol over the Au/TiO_2 catalysts with slight modification done from the earlier reported [39, 40].

These activity results suggest that 2 wt% Au/TiO_2 catalysts is found to be the best catalyst for the benzyl alcohol oxidation reaction in our present investigation. The reasons for faster deactivation of the above catalysts are probably due to low surface area, low gold dispersion and larger particle size employed during the reaction studies. The catalytic activity was well correlated with the particle size of gold on TiO_2 supports. The 1, 3 and 4 wt% Au/TiO_2 catalysts exhibits low catalytic activity compared to 2 wt% Au/TiO_2 catalyst and it can be attributed to the decrease in the number of active sites of gold on TiO_2 due to agglomeration of gold nanoparticles as evidenced from XRD, TEM and CO-chemisorption results.

4 Conclusions

Gold nanoparticles supported on mesoporous TiO_2 catalysts are found to be highly active for the vapor phase oxidation of benzyl alcohol to benzaldehyde. Moreover, high selectivity towards the formation of benzaldehyde makes gold as a promising catalyst for oxidation of benzyl alcohol reaction. XRD and pore size distribution results confirm that the pore structure of TiO_2 remains intact even after the introduction of gold. XRD results show that the presence of metallic gold nanoparticles. The catalyst with 2 wt% gold is found to be optimum loading for the conversion of benzyl alcohol beyond which the particle size of gold increases leading to decrease in the number of active sites and decrease in catalytic activity. The prepared catalysts showed remarkable catalytic activity for oxidation of benzyl alcohol under relatively mild conditions. The Au/TiO_2 catalysts were found to be an effective, reusable, and easily separated heterogeneous catalysts for oxidation of benzyl alcohol. These results also further supported by the TEM and CO-chemisorption measurements. XPS results reveal the formation of Au(0) after reduction with $NaBH_4$. The CO-chemisorption and BzOH activity studies infer that the gold dispersion, metal area and the oxidation activity of benzyl alcohol are related to one another.

Acknowledgments Ashish Kumar thanks Council of Scientific and Industrial Research (CSIR), New Delhi, India, for the award of Senior Research Fellowship (SRF).

References

1. Carrettin S, Concepcion P, Corma A, Nieto JML, Puntes VF (2004) Angew Chem Int Ed 43:2538–2540
2. Haruta M, Tsubota S, Kobayashi T, Kageyama H, Genet MJ, Delmon B (1993) J Catal 144:175–192
3. Pina CD, Falletta E, Rossi M (2008) J Catal 260:384–386
4. Mallat T, Baiker A (2004) Chem Rev 104:3037–3058
5. Enache DI, Edwards JK, Landon P, Solsona-Espriu B, Carley AF, Herzing AA, Watanabe M, Kiely CJ, Knight DW, Hutchings GJ (2006) Science 311:362–365
6. Haruta M (2002) Cattech 6:102–115
7. Enache DI, Knight DW, Hutchings GJ (2005) Catal Lett 103:43–52
8. Choudhary VR, Dumbre DK (2009) Top Catal 52:1677–1687
9. Biella S, Rossi M (2003) Chem Commun 21:378–379
10. Choudhary VR, Dumbre DK, Bhargava SK (2009) Ind Eng Chem Res 48:9471–9478
11. Chen Y, Lim H, Tang Q, Gao Y, Sun T, Yan Q, Yang Y (2010) Appl Catal A 380:55–65
12. Yu J, Qi L, Jaroniec M (2010) J Phys Chem C 114:13118–13125
13. Li HX, Bian ZF, Zhu J, Zhang DQ, Li GS, Huo YN, Li H, Lu YF (2007) J Am Chem Soc 129:8406–8407
14. Chen X (2009) Chin J Catal 30:839–851
15. Tian Y, Tatsuma T (2005) J Am Chem Soc 127:7632–7637
16. Iliev V, Tomova D, Bilyarska L, Tyuliev G (2007) J Mol Catal A 263:32–38
17. Chen DH, Huang FZ, Cheng YB, Caruso RA (2009) Adv Mater 21:2206–2210
18. Tran ND, Besson M, Descorne C (2011) New J Chem 35:2095–2104
19. Lopez N, Nørskov JK, Janssens TVW, Carlsson A, Molina AP, Clausen BS, Grunwaldt JD (2004) J Catal 225:86–94
20. Tsubota S, Haruta M, Kobayashi T, Ueda A, Nakahara Y (1991) Stud Surf Sci Catal 63:695–704
21. Widmann D, Behm RJ (2011) Angew Chem Int Ed 50:10241–10245
22. Addamo M, Augugliaro V, Paola AD, García-López E, Loddo V, Marcì G, Molinari R, Palmisano L, Schiavello M (2004) J Phys Chem B 108:3303–3310
23. Cui FM, Hua ZL, Wei CY, Li JQ, Gao Z, Shi JL (2009) J Mater Chem 19:7632–7637
24. Dimitratos N, Lopez-Sanchez JA, Morgan D, Carley A, Prati L, Hutchings GJ (2007) Catal Today 122:317–324
25. Srinivasu P, Singh SP, Islam A, Han L (2011) Adv Opt Electron 2011:1–5
26. Chen Y, Wang H, Liu CJ, Zeng Z, Zhang H, Zhou C, Jia X, Yang Y (2012) J Catal 289:105–117
27. Niwa M, Iwamoto M, Segawa K (1986) Bull Chem Soc Jpn 59:3735–3739
28. Yang HW, Tang DL, Lu XN, Yuan YZ (2009) J Phys Chem C 113:8186–8193
29. Yu JG, Su YR, Cheng B (2007) Adv Funct Mater 17:1984–1990
30. Flego C, Carluccio L, Rizzo C, Perego C (2001) Catal Commun 2:43–48
31. Du M, Zhan G, Yang X, Wang H, Lin W, Zhou Y, Zhu J, Lin L, Huang J, Sun D, Jia L, Li Q (2011) J Catal 283:192–201
32. Zwijnenburg A, Goossens A, Sloof WG, Crajé MWJ, Kraan AMVD, Jongh LJD, Makkee M, Moulijn JA (2002) J Phys Chem B 106:9853–9862
33. Kumar A, Sreedhar B, Chary KVR (2014) J Nanosci Nanotechnol 14:1–11
34. Choudhary VR, Chaudhari PA, Narkhede VS (2003) Catal Commun 4:171–175
35. Sankar M, He Q, Morad M, Pritchard J, Freakley SJ, Edwards JK, Taylor SH, Morgan DJ, Carley AF, Knight DW, Kiely CJ, Hutchings GJ (2012) ACS Nano 6:6600–6613
36. Sankar M, Nowicka E, Tiruvalam R, He Q, Taylor SH, Kiely CJ, Bethell D, Knight DW, Hutchings GJ (2011) Chem Eur J 17:6524–6532
37. Sankar M, Nowicka E, Miedziak PJ, Brett GL, Jenkins RL, Dimitratos N, Taylor SH, Knight DW, Bethell D, Hutchings GJ (2010) Faraday Discuss 145:341–356
38. Cao E, Sankar M, Nowicka E, He Q, Morad M, Miedziak PJ, Taylor SH, Knight DW, Bethell D, Kiely CJ, Gavriilidis A, Hutchings GJ (2013) Catal Today 203:146–152
39. Wang H, Fan W, He Y, Wang J, Kondo JN (2013) J Catal 299:10–19
40. Chen YT, Zheng HJ, Guo Z, Zhou CM, Wang C, Borgna A, Yang YH (2011) J Catal 283:34–44